Journal of Solid Mechanics Vol. 11, No. 2 (2019) pp. 236-253
DOI: 10.22034/JSM.2019.665162

Size-Dependent Analysis of Orthotropic Mindlin Nanoplate on Orthotropic Visco-Pasternak Substrate with Consideration of Structural Damping

A. Ghorbanpour Arani [1, 2 *], M.H. Jalaei [1], S. Niknejad [1], A.A. Ghorbanpour Arani[3]

[1]*Faculty of Mechanical Engineering, University of Kashan, Kashan, Iran*
[2]*Institute of Nanoscience & Nanotechnology, University of Kashan, Kashan, Iran*
[3]*School of Mechanical Engineering, College of Engineering, University of Tehran, Tehran, Iran*

Received 18 January 2019; accepted 23 March 2019

ABSTRACT

This paper discusses static and dynamic response of nanoplate resting on an orthotropic visco-Pasternak foundation based on Eringen's nonlocal theory. Graphene sheet modeled as nanoplate which is assumed to be orthotropic and viscoelastic. By considering the Mindlin plate theory and viscoelastic Kelvin-Voigt model, equations of motion are derived using Hamilton's principle which are then solved analytically by means of Fourier series -Laplace transform method. The parametric study is thoroughly accomplished, concentrating on the influences of size effect, elastic foundation type, structural damping, orthotropy directions and damping coefficient of the foundation, modulus ratio, length to thickness ratio and aspect ratio. Results depict that the structural and foundation damping coefficients are effective parameters on the dynamic response, particularly for large damping coefficients, where response of nanoplate is damped rapidly.

Keywords : Nonlocal static and dynamic response; Orthotropic nanoplate and foundation; Fourier series-Laplace transform; Structural and external damping.

1 INTRODUCTION

GRAPHENE SHEETS (GSs) as nanoplates are one atom thick two-dimensional layers of sp^2-bonded carbon densely packed to form a honeycomb crystal lattice. Especial properties of graphene sheets such as high strength, the low ratio of weight to area unit and extraordinary electrical properties, attracted many researchers to consider this topic as their major activities [1, 2]. It is studied the possibility of using graphene in magnetic sensor [3], nanocomposites [4], transistors [5], mass and gas sensors [6, 7], cellular photographing [8] and so on. There are different methods to analyze the nano structures known as molecular dynamics (MD) simulations, experimental study and continuum mechanics approach. Since performance and control of experiments and atomic modelling on the nano-scale level is difficult and expensive in computations, the continuum mechanics method is attended by many researchers in comparison with two other methods. Inasmuch as the classical continuum mechanics have no

*Corresponding author. Tel.: +98 31 55912450; Fax: +98 31 55912424.
E-mail address: aghorban@kashanu.ac.ir (A.Ghorbanpour Arani).

ability in capturing the small scale effects, it cannot be regarded as a reliable theory to predict the mechanical behavior of nanomaterials. So far, several nonclassical continuum theories have been formulated to incorporate the small-scale size effects in micro/nano structures, such as strain gradient theory [9], couple stress theory [10, 11] and nonlocal elasticity theory [12]. Among these size-dependent theories, the Eringen nonlocal elasticity theory is widely used in the study of structures at small scale. Eringen theory by considering the small scale effects, explains that the stress in a reference point is affected by the strains in whole body domain or the interactive bonds between the carbon atoms are not neglected and have significant effects in nano scales. The literature shows that nonlocal theory is being increasingly utilized for reliable and quick analysis of nanostructures in recent years. In this regard, a number of research works have been performed based on this theory in order to study on mechanical behavior of graphene sheets. Pradhan and Murmu [13] studied buckling analysis of biaxially compressed single-layered graphene sheet (SLGS) using the differential quadrature method (DQM). They found that buckling load decreases with increasing the nonlocal parameter. Hosseini Hashemi and Tourki Samaei [14] investigated the buckling of rectangular graphene plates using the Mindlin and Eringen nonlocal elasticity theories. They concluded that both nonlocal parameter and shear deformation are less important in lower buckling modes, and they are strongly important at higher buckling modes. Shen [15] investigated bending, vibrations and post buckling of rectangular graphene plates resting on elastic foundation, using classical plate theory (CLPT) by considering the nonlinear strains field in thermal environment. Ansari and Rouhi [16] proposed an analytical solution to calculate the critical buckling load for a monolayer graphene sheet under uniform loading by employing Galerkin method. Mohammadi et al. [17] studied free transverse vibration analysis of circular and annular graphene sheets using nonlocal continuum mechanics for various types of boundary conditions. They found that nondimensional frequency increases with increasing the radius for all mode numbers. Zenkour and Sobhy [18] investigated the thermal buckling of SLGS embedded in an elastic Winklere-Pasternak matrix, using the sinusoidal shear deformation plate theory and compared the results with classical and first-order shear deformation theories. Ghorbanpour Arani et al. [19] investigated nonlinear vibration response of the coupled system of double-layered annular graphene sheets (CS-DLAGSs) embedded in a visco-Pasternak medium via DQM. They revealed that the frequency reduction percent (FRP) of in phase-in phase-in phase (III) and out phase-out phase-out phase (OOO) vibration state are maximum and minimum, respectively. Kanaipour [20] studied static bending analysis of nanoplate embedded on elastic foundation. The governing equations for the nonlocal Mindlin and Kirchhoff plate models were derived and then were solved numerically using DQM. He observed that by increasing the elastic stiffness, the displacement ratio increases. Mohammadi et al. [21] presented nonlocal theory to study the free vibration of orthotropic SLGS resting on a Pasternak foundation under shear in-plane load based on CLPT and used the combined Galerkin-DQM to solve the obtained equations. They concluded that small scale effects are more significant for the nanoplate with shear in-plane load compared to nanoplate without shear in-plane load. Golmakani and Rezatalab [22] presented the nonlinear bending analysis of rectangular orthotropic SLGS resting on Pasternak foundation based on nonlocal first order shear deformation theory (FSDT). Their results showed that when the elastic foundation exists, the linear to nonlinear deflection ratio decreases.

A close scrutiny of previous researches shows that only few works have (have) been devoted to dynamic analysis of nanoplate. In this regard, Liu and Chen [23] analyzed dynamic response of the finite periodic SLGSs with different boundary conditions using the wave method. Most recently, Ghorbanpour Arani and Jalaei [24] investigated static bending and dynamic behavior of embedded isotropic elastic SLGS based on nonlocal third-order shear deformation theory (TSDT). The surrounding medium was simulated by isotropic visco-Pasternak model. They revealed that when the nonlocal parameter increases, the dynamic response increases. Also, their results indicated that the small scale effect on the deflection is more prominent as the nanoplate becomes thicker and the aspect ratios increases. None of the research works which are mentioned above have modeled nanoplates as viscoelastic structures whereas the nanoplates reveal viscoelastic structural damping as many materials. Recently, Pouresmaeeli et al. [25] performed vibration analysis of a simply supported viscoelastic orthotropic nanoplate resting on viscoelastic foundation. They showed that increasing the structural damping and foundation damping coefficients diminishes the frequency of orthotropic nanoplates. Karličić et al. [26] carried out the free vibration of a viscoelastic orthotropic multi-nanoplate system (MNPS) by including the effect of viscoelastic foundation, based on the Kirchhoff plate theory. Wang et al. [27] presented analytical solutions for nonlinear vibration of the double layered viscoelastic nanoplates based on CLPT. Their results indicated that the Van der Waals interaction has considerable effects on the natural frequency, while the effect of the structural damping coefficient on the nonlinearity frequency is not significant. Hosseini Hashemi et al. [28] investigated the free transverse vibration of a nonlocal viscoelastic double graphene sheets (NVDGS) coupled with visco-Pasternak layer based on CLPT using exact solution. They showed that natural frequency and stability of the system rise as the Winkler and Pasternak coefficients increase and layer damping effect decreases.

However, to the best of authors' knowledge, no study has focused on static and dynamic bending of viscoelastic orthotropic SLGS resting on orthotropic visco-Pasternak foundation under sinusoidal and uniform loads so far. Considering viscoelastic characterization both GS and foundation are very significant for perfect analysis of NEMS. Hence, in this work an entirely analytical method to study the static and dynamic responses of SLGS with considering foundation effects is developed using the Fourier series-Laplace transform. Viscoelasticity of the structure material is modeled with parallel springs and dashpots as the Kelvin-Voigt model. The SLGS resting on the viscoelastic medium is simulated by orthotropic visco-Pasternak type as spring, shear and damping foundations with considering shear direction and orthotropy angle. Based on the Mindlin plate theory, equations of motion are derived employing Hamilton's principle. Furthermore, the nonlocal elasticity theory is applied to capture the small scale effects. Using Laplace transform, the time dependency of the governing equations is eliminated and then an analytical strategy is employed to invert the results into the time domain. Finally, the influences of small scale effect, modulus ratio, elastic foundation type, structural damping, orthotropy directions and damping coefficient of the foundation, loading type, length to thickness ratio and aspect ratio on the static and dynamic behavior of SLGS are discussed. The obtained results would be helpful while designing NEMS devices using GSs.

2 BASIC EQUATIONS

A schematic configuration of the viscoelastic orthotropic SLGS with length a, width b and thickness h resting on an orthotropic visco-Pasternak foundation subjected to dynamic transverse uniform and sinusoidal loads has been illustrated in Fig. 1. The viscoelastic nanoplate is described based on the Kelvin-Voigt model consists of an infinite set of springs and dashpots in parallel. This model handles the characteristics of creep and recovery fairly well. As shown, due to the presence of arbitrarily orthotropic foundation, the global coordinates of the nanoplate (x, y, z) will not coincide with the local orthotropy coordinates (ξ, η) of the medium.

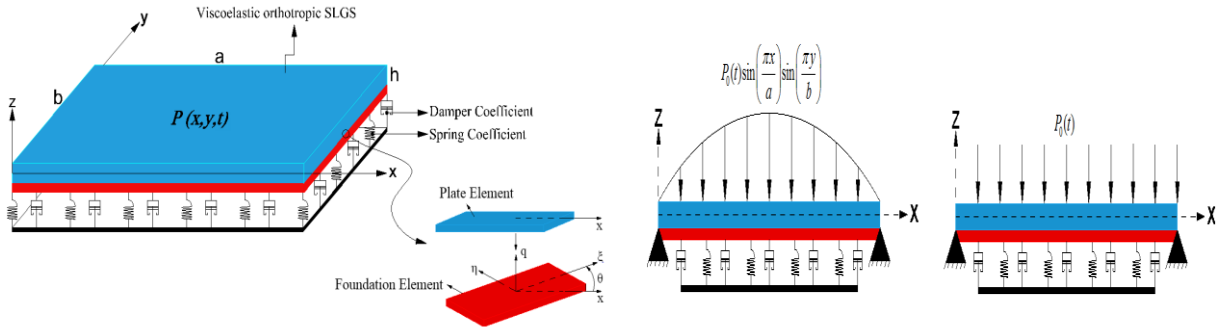

(a) (b)

Fig.1
a) Configuration of viscoelastic orthotropic SLGS resting on orthotropic visco-Pasternak foundation. b) Schematic of viscoelastic orthotropic SLGS under uniform and sinusoidal loads.

2.1 Nonlocal continuum theory

The conventional local theory is not size dependent theory. Thus, it is required to modify this theory to include small scale effects. For this purpose, nonlocal elasticity theory was suggested by Eringen [12]. Due to its efficiency and simplicity, it has been extensively applied. According to the nonlocal theory, the stress tensor at an arbitrary point in a body depends not only on the strain tensor at that point but also on the strain tensor at all other points of the body. This observation is in accordance with atomic theory of lattice dynamics and experimental observations on phonon dispersion. Using nonlocal elasticity theory, the constitutive equation for a linear homogenous nonlocal elastic body neglecting the body forces is given as:

$$\sigma_{ij}^{nl}(x) = \int_V \alpha(|x - x'|, \tau)\sigma_{ij}^{l}\, dV(x'), \qquad \forall x \in V \tag{1}$$

where σ_{ij}^{nl} and σ_{ij}^{l} are, the nonlocal and local stress tensors, respectively; The term $\alpha(|x-x'|,\tau)$ is the nonlocal modulus, which incorporates nonlocal effects into the constitutive equation at the reference point produced by the local strain at the source x'; $|x-x'|$ represents the distance between x and x' in the Euclidean form, and $\tau = e_0 a / l$ in which l is the external characteristic length (e.g., crack length, wavelength), a is an internal characteristic length of the material (e.g., length of C-C bond, lattice parameter, granular distance), and e_0 indicates constant appropriate to each material, and Consequently, $e_0 a$ is a constant parameter which is obtained with the experimental observations or MD simulation results. It should be noted that when $e_0 a$ is equal to zero, the nonlocal elasticity reduces to the local (classical) elastic model. The differential form of Eq. (1) can be written as:

$$\left(1-\mu\nabla^2\right)\sigma^{nl} = C:\varepsilon \tag{2}$$

In above equation, the parameter $\mu = (e_0 a)^2$ denotes the small scale effect on the response of structures in nanosize and $\nabla^2 = \partial^2/\partial x^2 + \partial^2/\partial y^2$ is the Laplacian operator in a Cartesian coordinate system. Also, C is the fourth order stiffness tensor, ':' represents the double dot product and ε is the strain tensor.

Using Eq. (2), the constitutive equation of the orthotropic nanoplate can be expressed as:

$$\begin{Bmatrix}\sigma_{xx}^{nl}\\ \sigma_{yy}^{nl}\\ \sigma_{yz}^{nl}\\ \sigma_{xz}^{nl}\\ \sigma_{xy}^{nl}\end{Bmatrix} - \mu\nabla^2\begin{Bmatrix}\sigma_{xx}^{nl}\\ \sigma_{yy}^{nl}\\ \sigma_{yz}^{nl}\\ \sigma_{xz}^{nl}\\ \sigma_{xy}^{nl}\end{Bmatrix} = \begin{bmatrix}C_{11} & C_{12} & 0 & 0 & 0\\ C_{21} & C_{22} & 0 & 0 & 0\\ 0 & 0 & C_{44} & 0 & 0\\ 0 & 0 & 0 & C_{55} & 0\\ 0 & 0 & 0 & 0 & C_{66}\end{bmatrix}\begin{Bmatrix}\varepsilon_{xx}\\ \varepsilon_{yy}\\ \gamma_{yz}\\ \gamma_{xz}\\ \gamma_{xy}\end{Bmatrix}. \tag{3}$$

The coefficients of C_{ij} are the plane stress-reduced stiffness of the orthotropic nanoplate defined as follow [29]:

$$C_{11} = \frac{E_1}{1-\nu_{12}\nu_{21}},\ C_{12} = \frac{\nu_{12}E_2}{1-\nu_{12}\nu_{21}},\ C_{22} = \frac{E_2}{1-\nu_{12}\nu_{21}},\ C_{66} = G_{23},\ C_{44} = G_{13},\ C_{55} = G_{12} \tag{4}$$

where E_1 and E_2 are the Young's moduli in directions x and y, respectively. G_{12}, G_{13} and G_{23} denote the shear moduli and ν_{12} and ν_{21} are the Poisson's ratios.

2.2 Strain displacement relationships

In this study, to capture the thickness shear deformations and rotary effects, the Mindlin plate theory (FSDT) is utilized to formulate the governing equations. Based on this theory, the mid-surface displacements (u_0, v_0, w_0), mid-surface rotations (ϕ_x, ϕ_y) and the displacement components of an arbitrary point (u, v, w) are in association as [29]:

$$\begin{aligned} u(x,y,z,t) &= u_0(x,y,t) + z\phi_x(x,y,t),\\ v(x,y,z,t) &= v_0(x,y,t) + z\phi_y(x,y,t),\\ w(x,y,z,t) &= w_0(x,y,t), \end{aligned} \tag{5}$$

In which t denotes the time variable.The linear in-plane and transverse shear strains are given by:

$$\begin{Bmatrix}\varepsilon_{xx}\\ \varepsilon_{yy}\\ \gamma_{xy}\end{Bmatrix}=\begin{Bmatrix}\varepsilon_{xx}^{(0)}\\ \varepsilon_{yy}^{(0)}\\ \gamma_{xy}^{(0)}\end{Bmatrix}+z\begin{Bmatrix}\varepsilon_{xx}^{(1)}\\ \varepsilon_{yy}^{(1)}\\ \gamma_{xy}^{(1)}\end{Bmatrix},\quad \begin{Bmatrix}\gamma_{yz}\\ \gamma_{xz}\end{Bmatrix}=\begin{Bmatrix}\gamma_{yz}^{(0)}\\ \gamma_{xz}^{(0)}\end{Bmatrix}, \tag{6}$$

where

$$\begin{Bmatrix}\varepsilon_{xx}^{(0)}\\ \varepsilon_{yy}^{(0)}\\ \gamma_{xy}^{(0)}\end{Bmatrix}=\begin{Bmatrix}u_{0,x}\\ v_{0,y}\\ u_{0,y}+v_{0,x}\end{Bmatrix},\quad \begin{Bmatrix}\varepsilon_{xx}^{(1)}\\ \varepsilon_{yy}^{(1)}\\ \gamma_{xy}^{(1)}\end{Bmatrix}=\begin{Bmatrix}\phi_{x,x}\\ \phi_{y,y}\\ \phi_{x,y}+\phi_{y,x}\end{Bmatrix},\quad \begin{Bmatrix}\gamma_{yz}^{(0)}\\ \gamma_{xz}^{(0)}\end{Bmatrix}=\begin{Bmatrix}\phi_{y}+w_{0,y}\\ \phi_{x}+w_{0,x}\end{Bmatrix}. \tag{7}$$

Here, the comma in subscript represents the partial differentiation.

3 ENERGY METHOD

3.1 Strain energy

The strain energy of the rectangular SLGS can be written as:

$$U=\frac{1}{2}\int_{-\frac{h}{2}}^{\frac{h}{2}}\int_0^b\int_0^a(\sigma_{xx}\varepsilon_{xx}+\sigma_{yy}\varepsilon_{yy}+K_s\sigma_{yz}\gamma_{yz}+K_s\sigma_{xz}\gamma_{xz}+\sigma_{xy}\gamma_{xy})\,dx\,dy\,dz \tag{8}$$

In the above equation, K_s is the shear correction factor of FSDT. As widely accepted, the approximate value of this quantity is $K_s=5/6$ [29].

3.2 Kinetic energy

The kinetic energy of the SLGS can be obtained as:

$$K=\frac{\rho h}{2}\int_0^b\int_0^a\left[(\dot{u})^2+(\dot{v})^2+(\dot{w})^2\right]dx\,dy \tag{9}$$

where ρ is the density of the orthotropic graphene sheet and dot-superscript convention shows the differentiation with respect to the time.

3.3 External works

The graphene sheet is subjected to the external applied loads and resting on an orthotropic visco-Pasternak elastic foundation. Hence, the external works can be divided to the following two distinct forces:

- Orthotropic visco-Pasternak medium
- External applied loads

3.3.1 Elastic medium

Winkler foundation or one-parameter model is the simplest simulation of a foundation that considers just the normal stresses. Pasternak foundation or two-parameter model considers not only the normal stresses, but also the transverse shear deformation. Taking the advantage of Pasternak's model, foundation can be defined generally as arbitrary orthotropy directions. Orthotropic visco-Pasternak foundation is simulated by adding damping to the orthotropic

Pasternak model. Since the damping coefficient has remarkable effect on the dynamic response of material, it should be considered in the dynamic analysis. Therefore, visco foundation can yield the accurate results with respect to non-visco ones. In this paper, the bottom surface of SLGS is continuously in contact with an orthotropic visco-Pasternak foundation. The force induced by orthotropic visco-Pasternak foundation can be obtained as [30, 31]:

$$F_1 = k_w w + c_d \dot{w} - k_{g\xi}(\cos^2\theta w_{,xx} + 2\cos\theta\sin\theta w_{,xy} + \sin^2\theta w_{,yy}) - k_{g\eta}(\sin^2\theta w_{,xx} - 2\sin\theta\cos\theta w_{,xy} + \cos^2\theta w_{,yy}) \quad (10)$$

In which k_w , c_d , $k_{g\xi}$ and $k_{g\eta}$ are spring, damper, ξ-shear and η-shear constants, respectively. The angle θ describes the local ξ direction of orthotropic foundation with respect to the global x-axis of the nanoplate.

3.3.2 External applied loads

The force due to external applied loads can be written as:

$$F_2 = -p \quad (11)$$

where p is the intensity of the distributed transverse load.

Therefore, the work done due to elastic medium and external forces on the SLGS is

$$V = -\frac{1}{2}\int_0^b \int_0^a (F_1 + F_2) w \, dx \, dy \quad (12)$$

4 EQUATIONS OF MOTION

Applying Hamilton's principle the variational form of motion equations can be expressed as follows:

$$\delta \int_0^t [K - (V + U)] \, dt = 0 \quad (13)$$

Equating the coefficients of δu_0 , δv_0 , δw_0 , $\delta \phi_x$ and $\delta \phi_y$ to zero, the following equations of motion can be obtained:

$$\delta u_0 : \; N_{xx,x} + N_{xy,y} = I_0 \ddot{u}_0 + I_1 \ddot{\phi}_x \; , \quad (14a)$$

$$\delta v_0 : \; N_{xy,x} + N_{yy,y} = I_0 \ddot{v}_0 + I_1 \ddot{\phi}_y \; , \quad (14b)$$

$$\delta w_0 : \; Q_{xz,x} + Q_{yz,y} + p(x,y,t) - k_w w_0 + k_{g\xi}(\cos^2\theta w_{0,xx} + 2\cos\theta\sin\theta w_{0,xy} + \sin^2\theta w_{0,yy}) + k_{g\eta}(\sin^2\theta w_{0,xx} - 2\sin\theta\cos\theta w_{0,xy} + \cos^2\theta w_{0,yy}) = I_0 \ddot{w}_0 + c_d \dot{w}_0 \; , \quad (14c)$$

$$\delta \phi_x : \; M_{xx,x} + M_{xy,y} - Q_{xz} = I_1 \ddot{u}_0 + I_2 \ddot{\phi}_x \; , \quad (14d)$$

$$\delta \phi_y : \; M_{xy,x} + M_{yy,y} - Q_{yz} = I_1 \ddot{v}_0 + I_2 \ddot{\phi}_y \; , \quad (14e)$$

where

$$\begin{Bmatrix} N_{\alpha\beta} \\ M_{\alpha\beta} \end{Bmatrix} = \int_{-\frac{h}{2}}^{\frac{h}{2}} \sigma_{\alpha\beta}^{nl} \begin{Bmatrix} 1 \\ z \end{Bmatrix} \mathrm{dz} \quad \alpha = x, y \quad \beta = x, y \tag{15a}$$

$$Q_{\alpha z} = K_s \int_{-\frac{h}{2}}^{\frac{h}{2}} \sigma_{\alpha z}^{nl} \, \mathrm{dz} \quad \alpha = x, y \tag{15b}$$

$$I_i = \rho \int_{-h/2}^{h/2} z^i dz \quad (i = 0,1,2), \tag{15c}$$

In which $N_{\alpha\beta}$, $M_{\alpha\beta}$ and $Q_{\alpha z}$ are in-plane, moment and transverse shear stress resultants of nonlocal elasticity, respectively.

The stress resultants are related to the strains as follows:

$$\begin{Bmatrix} \{N\} \\ \{M\} \end{Bmatrix} - \mu\nabla^2 \begin{Bmatrix} \{N\} \\ \{M\} \end{Bmatrix} = \begin{bmatrix} [A] & [0] \\ [0] & [D] \end{bmatrix} \begin{Bmatrix} \{\varepsilon^{(0)}\} \\ \{\varepsilon^{(1)}\} \end{Bmatrix}, \tag{16a}$$

$$\begin{Bmatrix} \{Q_{yz}\} \\ \{Q_{xz}\} \end{Bmatrix} - \mu\nabla^2 \begin{Bmatrix} \{Q_{yz}\} \\ \{Q_{xz}\} \end{Bmatrix} = \begin{bmatrix} J_{44} & 0 \\ 0 & J_{55} \end{bmatrix} \begin{Bmatrix} \{\gamma_{yz}^{(0)}\} \\ \{\gamma_{xz}^{(0)}\} \end{Bmatrix}, \tag{16b}$$

where

$$\{N\} = \{N_{xx} \quad N_{yy} \quad N_{xy}\}^T, \ \{M\} = \{M_{xx} \quad M_{yy} \quad M_{xy}\}^T \tag{17a}$$

$$\{\varepsilon^{(0)}\} = \{\varepsilon_{xx}^{(0)} \quad \varepsilon_{yy}^{(0)} \quad \gamma_{xy}^{(0)}\}^T, \ \{\varepsilon^{(1)}\} = \{\varepsilon_{xx}^{(1)} \quad \varepsilon_{yy}^{(1)} \quad \gamma_{xy}^{(1)}\}^T \tag{17b}$$

Here A_{ij}, D_{ij} and J_{ii} which are the extensional, bending and shear stiffness of the graphene sheet defined as:

$$\left(A_{ij}, D_{ij}\right) = \int_{-h/2}^{h/2} C_{ij} \left(1, z^2\right) dz \qquad (i, j = 1,2,6), \tag{18a}$$

$$J_{ii} = K_s \int_{-h/2}^{h/2} C_{ii} \, dz = K_s h C_{ii} \qquad (i = 4,5) \tag{18b}$$

Kelvin-Voigt model is employed for considering viscoelastic behavior of the nanostructure. According to this model, Young's moduli E_i and shear moduli G_{ij} are as follows [25]:

$$E_i = E_i \left(1 + g \frac{\partial}{\partial t}\right) \qquad (i = 1,2), \tag{19a}$$

$$G_{ij} = G_{ij} \left(1 + g \frac{\partial}{\partial t}\right) \qquad (i \neq j = 1,2,3) \tag{19b}$$

In which g is the structural damping coefficient. Substituting Eqs. (15), (18) and (19) into the equations of motion (i.e., Eq. (14)), the governing equations of viscoelastic orthotropic SLGS in terms of displacements and rotations can be obtained as:

$$\bar{A}_1(u_{0,xx}+g\dot{u}_{0,xx})+\bar{A}_2(u_{0,yy}+g\dot{u}_{0,yy})+\bar{A}_3(v_{0,xy}+g\dot{v}_{0,xy})+(1-\mu\nabla^2)(\bar{A}_4\ddot{u}_0+\bar{A}_5\ddot{\phi}_x)=0, \tag{20a}$$

$$\bar{B}_1(u_{0,xy}+g\dot{u}_{0,xy})+\bar{B}_2(v_{0,xx}+g\dot{v}_{0,xx})+\bar{B}_3(v_{0,yy}+g\dot{v}_{0,yy})+(1-\mu\nabla^2)(\bar{B}_4\ddot{v}_0+\bar{B}_5\ddot{\phi}_y)=0, \tag{20b}$$

$$\begin{aligned}&\bar{C}_1(w_{0,xx}+gw\dot{}_{0,xx})+\bar{C}_2(w_{0,yy}+gw\dot{}_{0,yy})+\bar{C}_3(\phi_{x,x}+g\dot{\phi}_{x,x})+\bar{C}_4(\phi_{y,y}+g\dot{\phi}_{y,y})\\&+(1-\mu\nabla^2)\begin{pmatrix}\bar{C}_5\ddot{w}_0-k_w w_0+k_{g\xi}(\cos^2\theta\, w_{0,xx}+2\cos\theta\sin\theta\, w_{0,xy}+\sin^2\theta\, w_{0,yy})\\+k_{g\eta}(\sin^2\theta\, w_{0,xx}-2\sin\theta\cos\theta\, w_{0,xy}+\cos^2\theta\, w_{0,yy})-c_d w\dot{}_0+p(x,y,t)\end{pmatrix}=0,\end{aligned} \tag{20c}$$

$$\begin{aligned}&\bar{D}_1(w_{0,x}+gw\dot{}_{0,x})+\bar{D}_2(\phi_{x,xx}+g\dot{\phi}_{x,xx})+\bar{D}_3(\phi_{x,yy}+g\dot{\phi}_{x,yy})+\bar{D}_4(\phi_x+g\dot{\phi}_x)+\bar{D}_5(\phi_{y,xy}+g\dot{\phi}_{y,xy})\\&+(1-\mu\nabla^2)(\bar{D}_6\ddot{u}_0+\bar{D}_7\ddot{\phi}_x)=0,\end{aligned} \tag{20d}$$

$$\begin{aligned}&\bar{E}_1(w_{0,y}+gw\dot{}_{0,y})+\bar{E}_2(\phi_{x,xy}+g\dot{\phi}_{x,xy})+\bar{E}_3(\phi_{y,xx}+g\dot{\phi}_{y,xx})+\bar{E}_4(\phi_{y,yy}+g\dot{\phi}_{y,yy})+\bar{E}_5(\phi_y+g\dot{\phi}_y)\\&+(1-\mu\nabla^2)(\bar{E}_6\ddot{v}_0+\bar{E}_7\ddot{\phi}_y)=0,\end{aligned} \tag{20e}$$

where the coefficients $\bar{A}_i$, $\bar{B}_i$, $\bar{C}_i$, $\bar{D}_i$, and $\bar{E}_i$ are given in Appendix A.

Considering that the rectangular graphene sheet has simply supported boundary conditions at all four edges, we can write following form [29]:

$$u_0(x,0,t)=0,\quad \phi_x(x,0,t)=0,\quad u_0(x,b,t)=0,\quad \phi_x(x,b,t)=0, \tag{21a}$$

$$v_0(0,y,t)=0,\quad \phi_y(0,y,t)=0,\quad v_0(a,y,t)=0,\quad \phi_y(a,y,t)=0, \tag{21b}$$

$$w_0(x,0,t)=0,\quad w_0(x,b,t)=0,\quad w_0(0,y,t)=0,\quad w_0(a,y,t)=0, \tag{21c}$$

$$N_{xx}(0,y,t)=0,\quad N_{xx}(a,y,t)=0,\quad N_{yy}(x,0,t)=0,\quad N_{yy}(x,b,t)=0, \tag{21d}$$

$$M_{xx}(0,y,t)=0,\quad M_{xx}(a,y,t)=0,\quad M_{yy}(x,0,t)=0,\quad M_{yy}(x,b,t)=0, \tag{21e}$$

5 SOLUTION PROCEDURE

5.1 Space solution

A closed-form Navier's type solution is employed to solve governing equations. On the basis of Navier solution, the generalized displacements are expanded in a double Fourier series as product of undetermined coefficients and known trigonometric functions to satisfy boundary conditions, i.e., Eq. (21). Hence, the appropriate displacement components can be defined as:

$$u_0(x,y,t)=\sum_{m=1}^{\infty}\sum_{n=1}^{\infty}U_{mn}(t)\cos(\alpha x)\sin(\beta y), \tag{22a}$$

$$v_0(x,y,t)=\sum_{m=1}^{\infty}\sum_{n=1}^{\infty}V_{mn}(t)\sin(\alpha x)\cos(\beta y), \tag{22b}$$

$$w_0(x,y,t)=\sum_{m=1}^{\infty}\sum_{n=1}^{\infty}W_{mn}(t)\sin(\alpha x)\sin(\beta y), \tag{22c}$$

$$\phi_x(x,y,t)=\sum_{m=1}^{\infty}\sum_{n=1}^{\infty}X_{mn}(t)\cos(\alpha x)\sin(\beta y), \tag{22d}$$

$$\phi_y(x,y,t)=\sum_{m=1}^{\infty}\sum_{n=1}^{\infty}Y_{mn}(t)\sin(\alpha x)\cos(\beta y), \tag{22e}$$

where $\alpha=\frac{m\pi}{a}$, $\beta=\frac{n\pi}{b}$, and *m, n* are the half wave numbers in the *x* and *y* directions, respectively.

Furthermore, as mentioned, it is assumed that the nanoplate is subjected to transverse mechanical load which can be expressed as the following Fourier sin expansion:

$$p(x,y,t)=\sum_{m=1}^{\infty}\sum_{n=1}^{\infty}p_{mn}(t)\sin(\alpha x)\sin(\beta y) \tag{23}$$

Here, the coefficients $p_{mn}(t)$ for two types of dynamic load distribution at the top surface of viscoelastic orthotropic SLGS are presented as:

$$\begin{aligned} &p_{mn}(t)=\frac{16P(t)}{mn\pi^2}, \quad (m,n=1,3,5,...) && \text{for uniform load}\\ &p_{mn}(t)=P(t), \quad (m=n=1) && \text{for sinusoidal load}\end{aligned} \tag{24}$$

where $P(t)=P_0H(t)$, and P_0 represents the intensity of distributed applied load. Also, $H(t)$ is the Heaviside step function defined as $H(t)=\begin{cases}1, & t\geq 0\\ 0, & t<0\end{cases}$.

Substituting Eqs. (22) and (23) into the governing Eq.(20), the following system of equations is obtained in a matrix form as:

$$[M_{mn}]\{\ddot{\Delta}_{mn}\}+[C_{mn}]\{\dot{\Delta}_{mn}\}+[K_{mn}]\{\Delta_{mn}\}=\{F_{mn}\}, \tag{25}$$

In which $\{\Delta_{mn}\}=\{U_{mn}\ \ V_{mn}\ \ W_{mn}\ \ X_{mn}\ \ Y_{mn}\}^T$ is the displacement vector. Furthermore, the $[M],[C]$ and $[K]$ are the mass, damping and stiffness matrices, respectively, which are defined in Appendix B.

5.2 Dynamic response solutions

For the dynamic bending analysis, Eq. (25) must be solved by using the Laplace transformation. Performing the Laplace transform on Eq. (25) and considering zero initial conditions at the initial time (namely, $\{\Delta_{mn}\}=\{\dot{\Delta}_{mn}\}=0$ at $t=0$), yields a new system of equations in which time dependency is eliminated as follows:

$$\left[K_{mn}+sC_{mn}+s^2M_{mn}\right]\{\bar{\Delta}_{mn}\}=\{\bar{F}_{mn}\}, \tag{26}$$

Here, s is the Laplace transform parameter and the bar superscript indicates transformed quantities.

5.3 Analytical Laplace inversion

At the end of previous section, each of the five components of the displacement vector was obtained in the Laplace domain. In this section, an analytical Laplace inversion technique is employed to return the displacement vector from Laplace domain into the real time domain.

A function $\hat{f}(s)=\dfrac{A(s)}{B(s)}$ can be used to find the unknown variables in Eq. (26) in the Laplace transformation domain. Both functions $A(s)$ and $B(s)$ are in the form of polynomials. Let's suppose that the roots of the function $B(s)$ are known. Some of the roots are real roots which are denoted by r_i and the others are complex and indicated by c_i . Number of r_i and c_i are shown as n_r and n_c , respectively. When all roots are simple, the inverse of the function $\hat{f}(s)$, that is $f(t)$, is obtained as [32, 33]:

$$f(t)=Re\left(\sum_{i=1}^{n_c}\frac{A(c_i)}{B'(c_i)}e^{c_i t}\right)+\sum_{j=1}^{n_r}\frac{A(r_j)}{B'(r_j)}e^{r_j t}. \tag{27}$$

where $Re(x)$ denotes the real part of the complex number x and the prime specifies a derivative with respect to s. Following the mentioned approach, each component of the displacement vector is derived analytically.

6 NUMERICAL RESULTS AND DISCUSSION

In this study, static deflection and dynamic response of orthotropic SLGS is carried out. The effects of various parameters such as small scale parameter, material properties, structural damping, viscoelastic foundation, kind of the applied load, length to thickness ratio (*a/h*) and aspect ratio (*a/b*) are presented. Since the successful application of the nonlocal continuum mechanics requires to determine the magnitude of the small scale parameter e_0a , an appropriate choice of this parameter had to be made. In the most studies e_0 is usually taken to be 0.39 proposed by Eringen [12]. Literatures show that the magnitudes of e_0 extremely depend on various parameters, and its actual value is not known so far. Some researchers assumed a range of values $e_0a=0.2nm$ for different analyses of GS [16, 30]. So in this research, the values of small scale parameter μ are taken as zero up to 4 nm^2. Geometrical and material properties of the isotropic and orthotropic SLGS are presented in Table1.

Table 1
Geometrical and material properties of the isotropic and orthotropic SLGS [34].

Elastic properties	Isotropic graphene sheet	Orthotropic graphene sheet
E_1 (GPa)	1060	1765
E_2 (GPa)	1060	1588
ν_{12}	0.25	0.30
ν_{21}	0.25	0.27
ρ (kg/m^3)	2250	2300
h (nm)	0.34	0.34

6.1 Verification studies

To show the accuracy and efficiency of the proposed method in static bending and dynamic response, some comparison studies are presented in Table 2., as well as in Fig. 2.

6.1.1 Static deflection of orthotropic plate

As an example, the non-dimensional defection of orthotropic plates under uniformly distributed load without considering both the effects of elastic medium and nonlocal parameter are compared with those available in [35] based on two-variable plate theory (TVPT). The used material properties are taken as: $E_1/E_2 = E_r$ varied, $G_{12}/E_2 = G_{13}/E_2 = 0.6$, $G_{23}/E_2 = 0.5$, $\nu_{12} = 0.25$. A brief review of Table 2., shows that the present deflection is in good agreement with the results in literature.

Table 2
Comparison of non-dimensional deflection $\bar{w}$ of orthotropic plate under uniform load.

E_r	*a/b*	*a/h=10*		*a/h=100*	
		TVPT [35]	Present	TVPT [35]	Present
10	0.5	1.8218	1.8311	1.5886	1.5775
	1	1.5334	1.5489	1.3739	1.3736
	2	0.5847	0.5967	0.5190	0.5190
20	0.5	1.0313	1.0411	0.7983	0.7877
	1	0.9445	0.9576	0.7851	0.7851
	2	0.4775	0.4805	0.4118	0.4121

6.1.2 Dynamic response of FGM plates

To the best of authors' knowledge no published literature is available for dynamic response of viscoelastic orthotropic SLGS resting on the orthotropic visco-Pasternak foundation. Since no reference to such a work is found to data in the literature, its verification is not possible. However, in an attempt to validate this study, a simplified analysis of this work is done without considering the size effect, elastic foundation and orthotropic and viscoelastic properties of the nanoplate. In Fig. 2, the present results are compared with the work of Reddy [36] who analyzed functionally graded material (FGM) plate under a uniformly distributed load based on the finite element method (FEM). For this purpose, the geometric properties are assumed to be: a=b=0.2 m, h=0.01 m and loading intensity is P_0=106 N/m^2. Also, the central deflection and time are normalized as $w^* = w_c h E_m / a^2 P_0$ and $t^* = t\sqrt{E_m / a^2 \rho_m}$, where E_m and ρ_m are the corresponding properties of the metal. As observed, in this case, our outcomes agree excellent with the finite elements results.

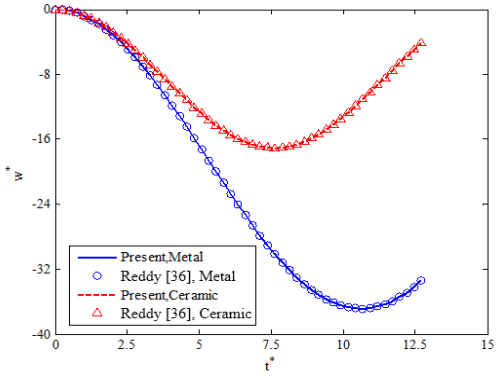

Fig.2
Comparison between deflection time-history of the center of FG square plate under the uniform load.

6.2 Parametric studies

For convenience, the following non-dimensional parameters are used in presenting the numerical results:

$$w^* = \frac{w_c h E_2}{b^2 P_0}, \quad K_W = \frac{k_w a^4}{D_{11}}, \quad K_{G\xi} = \frac{k_{g\xi} a^2}{D_{11}}, \quad K_{G\eta} = \frac{k_{g\eta} b^2}{D_{11}}$$
$$C_D = \frac{c_d a^2}{\sqrt{\rho h D_{11}}}, \quad G = \frac{g}{a^2}\sqrt{\frac{D_{11}}{\rho h}}, \quad t^* = t\sqrt{\frac{E_2}{b^2\rho}}, \quad D_{11} = \frac{E_1 h^3}{12\left(1-\nu_{12}\nu_{21}\right)} \tag{28}$$

The values of the length to thickness ratio and aspect ratio are assumed to be 10 and 1, respectively, unless otherwise stated. Also, magnitude of the applied load is P_0=10^6 N/m^2.

6.2.1 Static analysis of orthotropic nanoplate

At first, the effect of aspect ratio, length-to-thickness ratio and nonlocal parameter on the non-dimensional central deflections of orthotropic nanoplate without foundation under sinusoidally and uniformly distributed transverse loads is investigated in Table 3. Central deflection is normalized and is indicated by $w^* = 100 w_c h^3 E_2 / a^4 P_0$. It is obvious that the nonlocal parameter μ is a significant parameter in the analysis of nanomaterials and should not be neglected in the nanostructure. As can be seen that the amplitude of deflection increases when the nonlocal parameter increases. It is need to point out that the zero value for nonlocal parameter (i.e., μ=0) denotes the results obtained by the local elasticity theory which has the lowest deflection. It is also observed that non-dimensional maximum deflection decreases with the increase in aspect ratio. Furthermore, it can be seen that the small scale parameter has a slight effect on the deflection as the length to thickness ratio increases. Finally, it can be observed that deflection for uniform loading is obtained more than sinusoidal loading.

Table 3
The non-dimensional deflections of orthotropic nanoplate under sinusoidal and uniform loads for various values of the aspect ratio, length to thickness ratio and nonlocal parameter.

a/b	*a/h*	$\mu(nm^2)$	Loading	
			UL	SL
1	10	0	4.3733	2.7744
		1	11.1239	7.5119
		2	17.8745	12.2494
	100	0	4.1848	2.6447
		1	4.2503	2.6899
		2	4.3158	2.7350
2	10	0	0.7469	0.4884
		1	3.5732	2.5733
		2	6.3994	4.6582
	100	0	0.6787	0.4393
		1	0.7051	0.4581
		2	0.7316	0.4768

Table 4., explains the non-dimensional central deflection of isotropic and orthotropic graphene sheet with or without elastic foundation for various values of nonlocal parameter subjected to sinusoidal loading. As can be seen, considering elastic medium decreases deflection of nanoplate. It is due to the fact that considering elastic medium leads to stiffer nanoplate. Furthermore, the effect of the Pasternak foundation (i.e. $K_W \neq 0$ and $K_G \neq 0$) is higher than the Winkler foundation (i.e. $K_W \neq 0$ and $K_G = 0$) for decreasing of the nanoplate. It is because Winkler foundation is capable to describe just normal load, while the Pasternak medium describes both normal and transverse shear loads. It is also concluded that with increasing the value of nonlocal parameter, the difference between the deflection of with and without foundation becomes more obvious. Consequently, existence of elastic foundation is an important factor for decreasing the deflection of the nanoplate and must be considered, especially in the higher nonlocal parameters. Further, from this table, it is found that the deflection of the isotropic nanoplate is always greater than of orthotropic one.

Table 4
The non-dimensional central deflection of isotropic and orthotropic graphene sheet with or without elastic foundation for different values of nonlocal parameter subjected to sinusoidal loading.

K_W	K_G	μ (nm^2)			
		1	2	3	4
0	0	8.2290	13.4187	18.6084	23.7981
100	0	4.7526	6.1195	7.0112	7.6388
100	10	2.5915	2.9509	3.1437	3.2640
0	0	7.5119	12.2494	16.9869	21.7244
100	0	4.2752	5.4818	6.2636	6.8113
100	10	2.3103	2.6222	2.7887	2.8922

6.2.2 Dynamic analysis of viscoelastic nanoplate resting on the visco-Pasternak foundation

In this section, dynamic response of viscoelastic orthotropic SLGS resting on orthotropic visco-Pasternak foundation is investigated graphically.

Fig. 3 demonstrates the effect of different elastic medium on the dynamic response of the orthotropic SLGS under sinusoidal load for μ=1 nm^2. As seen, when an elastic foundation is present, the dynamic response of the nanoplate is diminished in comparison without the foundation condition. Furthermore, it is observed that the effect of the Pasternak foundation is higher than the Winkler foundation for decreasing the deflection amplitude of the nanoplate. It is also seen that the orthotropic Pasternak foundation is more effective than the isotropic Pasternak type to reduce the dynamic response of the nanoplate due to considering an arbitrarily oriented foundation.

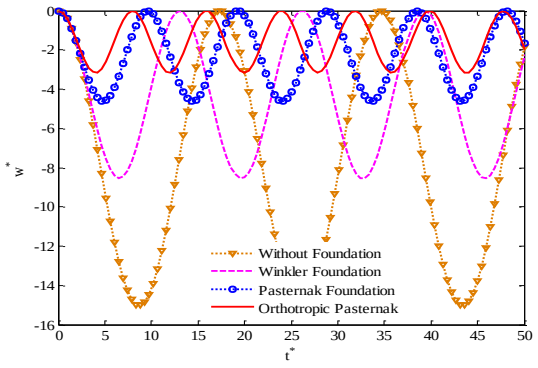

Fig.3
Effect of the elastic foundation type on dynamic response of an orthotropic SLGS under sinusoidal load for μ=1 nm^2.

The effect of orthotropy angle on the dynamic response of orthotropic nanoplate resting on orthotropic Pasternak foundation subjected to sinusoidal load is depicted in Fig. 4 for λ=2 in which $\lambda = K_{G\xi} / K_{G\eta}$. However, it should be noted that for λ=1 the foundation becomes isotropic Pasternak. The spring and η-shear constants are assumed as $K_W = 100$ and $K_{G\eta} = 10$, respectively, and the nonlocal parameter μ is considered to be 2 nm^2. Since the orthotropy angle of foundation can be affected the deflection of nanoplate, it is a significant factor. From this figure, it can be concluded that θ=45° is the best angle to obtain the minimum deflection among others.

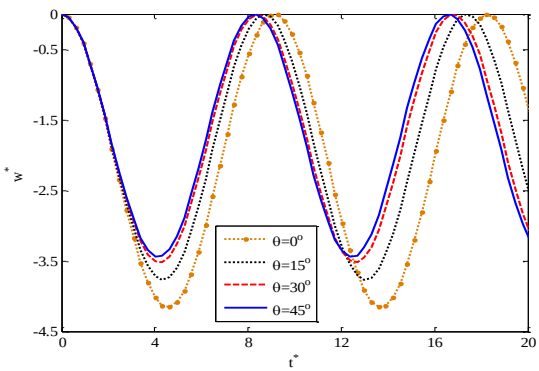

Fig.4
Effect of orthotropy angle on the dynamic response of orthotropic SLGS resting on orthotropic Pasternak foundation under sinusoidal load for λ=2.

For numerical calculations in the following figures, it is considered $K_W = 100$, $K_{G\eta} = 10$, $K_{G\xi} = 20$ and θ=45°. Moreover, the non-dimensional structural damping coefficient G and the non-dimensional damping constant of foundation C_D are taken to be 0.01 and 1, respectively (unless otherwise stated).

To show the effect of the damping coefficient of the orthotropic visco-Pasternak foundation on the dynamic response of viscoelastic orthotropic SLGS, three different values of the damping constant have been plotted in Fig. 5 under sinusoidal load for 3 nm^2. As seen, it is apparent that the deflection of nanoplate are strongly influenced by the damping coefficient of the medium C_D. Increasing the damping constant decreases the deflection and causes the response to reach the static response much faster.

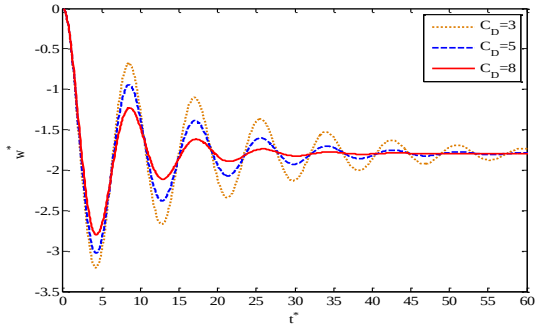

Fig.5
Deflection history of viscoelastic orthotropic SLGS for various values of the damping coefficient of foundation under sinusoidal load for μ=3 nm^2.

Fig. 6 indicates the effect of the different viscoelastic structural damping coefficients on the dynamic response of viscoelastic orthotropic nanoplate resting on orthotropic visco-Pasternak foundation subjected to sinusoidal load for 3 nm^2. It can be observed that the dynamic response is significantly influenced by the structural damping coefficient G. As expected, the deflection of the nanoplate decreases with increasing the structural damping coefficient.

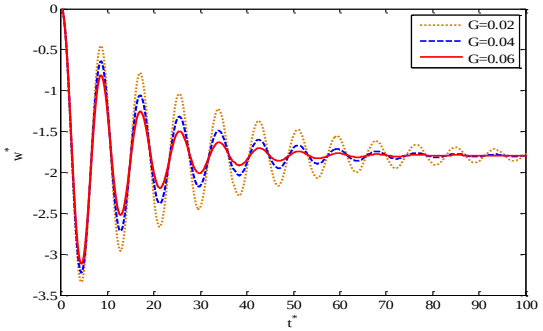

Fig.6
Effect of structural damping on the dynamic response of orthotropic SLGS resting on orthotropic visco-Pasternak foundation under sinusoidal load for μ=3 nm^2.

To clarify the influences of damping coefficient of viscoelastic foundation and structural damping of the nanoplate on the dynamic response of the SLGS under a sinusoidal load, Fig. 7 is presented with μ=4 nm^2. It can be observed that the dynamic response is significantly influenced by the structural damping coefficient G and the damping coefficient of the foundation C_D. It is interesting to note that since increasing the structural and foundation damping causes more absorption of energy by the system, the dynamic response decreases.

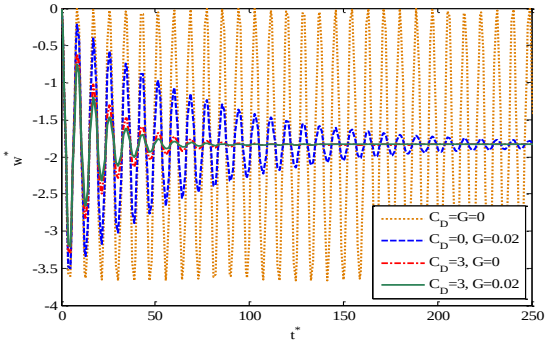

Fig.7
Coupled effects of the damping coefficient of visco-Pasternak foundation and structural damping of the nanoplate under sinusoidal load on the dynamic response for μ=4 nm^2.

Finally, Fig. 8 illustrates the influence of modulus ratio E_r on the dimensionless deflection of viscoelastic orthotropic SLGS resting on orthotropic visco-Pasternak medium subjected to sinusoidal for μ=4 nm^2. The used material properties are taken as: $E_r = E_1/E_2$ varied, $G_{12}=G_{13}=0.6\ E_2$, $G_{23}=0.5\ E_2$, $\nu_{12}=0.25$. It is seen that when the modulus ratio E_r increases, the deflection decreases and consequently the viscoelastic nanoplate reaches the equilibrium state much faster.

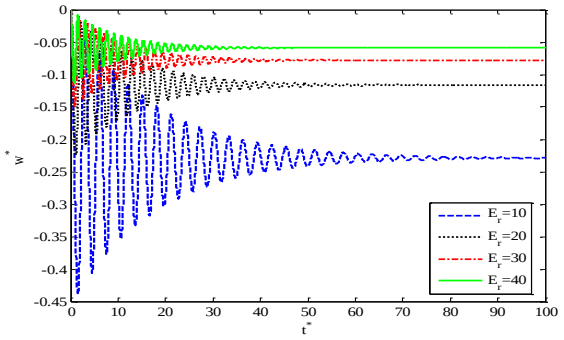

Fig.8
Influence of modulus ratio on the dimensionless deflection of viscoelastic orthotropic SLGS resting on orthotropic visco-Pasternak medium subjected to sinusoidal for μ=4 nm^2.

7 CONCLUSIONS

The present research was concerned with the size-dependent static and dynamic response of viscoelastic orthotropic SLGS embedded in an elastic medium under uniform and sinusoidal loads, for the first time. The kelvin-Voigt model was considered to describe the nanoplate viscoelasticity. The surrounding medium is simulated by orthotropic visco-Pasternak model. Based on the Mindlin plate theory, the nonlocal motion equations were derived via Hamilton's principle and then were solved analytically using Fourier series-Laplace transform technique for simply-supported boundary conditions. The total conclusions can be summarized as follows:

- The nonlocal parameter effect decreased extremely as length to thickness ratio increases.
- The presence of the elastic foundation increases the stiffness of the SLGS and therefore is a remarkable factor for decreasing the static deflection and dynamic response particularly in the higher nonlocal parameters.
- The orthotropic Pasternak medium with θ=45° is more effective than others for decreasing the deflection.
- Increasing modulus ratio leads to decreasing the static deflection and dynamic response of the orthotropic SLGS.
- Increasing the values of structure damping and foundation damping coefficients causes an obvious decrease of amplitude and time interval of response.

Finally, it is hoped that the results presented here can be utilized as benchmarks for verifying results obtained from the other mathematical approaches and also would be beneficial for the design of NEMS devices.

APPENDIX A

$$\bar{A}_1=\frac{E_1 h}{1-\nu_{12}\nu_{21}},\ \bar{A}_2=G_{12}h,\ \bar{A}_3=h\left(\frac{\nu_{12}E_2}{1-\nu_{12}\nu_{21}}+G_{12}\right),\ \bar{A}_4=-I_0,\ \bar{A}_5=-I_1 \tag{A.1}$$

$$\bar{B}_1=h\left(\frac{\nu_{12}E_2}{1-\nu_{12}\nu_{21}}+G_{12}\right),\ \bar{B}_2=G_{12}h,\ \bar{B}_3=\frac{E_2 h}{1-\nu_{12}\nu_{21}},\ \bar{B}_4=-I_0,\ \bar{B}_5=-I_1 \tag{A.2}$$

$$\bar{C}_1=K_s G_{13}h,\ \bar{C}_2=K_s G_{23}h,\ \bar{C}_3=K_s G_{13}h,\ \bar{C}_4=K_s G_{23}h,\ \bar{C}_5=-I_0 \tag{A.3}$$

$$\bar{D}_1 = -K_s G_{13} h,\ \bar{D}_2 = \frac{E_1 h^3}{12(1-\nu_{12}\nu_{21})},\ \bar{D}_3 = \frac{G_{12} h^3}{12},\ \bar{D}_4 = -K_s G_{13} h,\ \bar{D}_5 = \frac{h^3}{12}\left(\frac{\nu_{12} E_2}{1-\nu_{12}\nu_{21}} + G_{12}\right),\ \bar{D}_6 = -I_1,\ \bar{D}_7 = -I_2 \tag{A.4}$$

$$\bar{E}_1 = -K_s G_{23} h,\ \bar{E}_2 = \frac{h^3}{12}\left(\frac{\nu_{12} E_2}{1-\nu_{12}\nu_{21}} + G_{12}\right),\ \bar{E}_3 = \frac{G_{12} h^3}{12},\ \bar{E}_4 = \frac{E_2 h^3}{12(1-\nu_{12}\nu_{21})},\ \bar{E}_5 = -K_s G_{23} h,\ \bar{E}_6 = -I_1,\ \bar{E}_7 = -I_2 \tag{A.5}$$

APPENDIX B

The components of the matrices introduced in Eq. (25) can be expressed as follows:

$$\begin{aligned}
&M_{11} = \bar{A}_4\left(1+\mu\alpha^2+\mu\beta^2\right),\quad M_{12} = M_{13} = 0,\quad M_{14} = \bar{A}_5\left(1+\mu\alpha^2+\mu\beta^2\right),\quad M_{15} = 0,\\
&M_{21} = 0,\quad M_{22} = \bar{B}_4\left(1+\mu\alpha^2+\mu\beta^2\right),\quad M_{23} = M_{24} = 0,\quad M_{25} = \bar{B}_5\left(1+\mu\alpha^2+\mu\beta^2\right),\\
&M_{31} = M_{32} = 0,\quad M_{33} = \bar{C}_5\left(1+\mu\alpha^2+\mu\beta^2\right),\quad M_{34} = M_{35} = 0,\\
&M_{41} = \bar{D}_6\left(1+\mu\alpha^2+\mu\beta^2\right),\quad M_{42} = M_{43} = 0,\quad M_{44} = \bar{D}_7\left(1+\mu\alpha^2+\mu\beta^2\right),\quad M_{45} = 0,\\
&M_{51} = 0,\quad M_{52} = \bar{E}_6\left(1+\mu\alpha^2+\mu\beta^2\right),\quad M_{53} = M_{54} = 0,\quad M_{55} = \bar{E}_7\left(1+\mu\alpha^2+\mu\beta^2\right)
\end{aligned} \tag{B.1}$$

$$\begin{aligned}
&C_{11} = -g\left(\bar{A}_1\alpha^2+\bar{A}_2\beta^2\right),\quad C_{12} = -\alpha\beta\bar{A}_3 g,\quad C_{13} = C_{14} = C_{15} = 0,\\
&C_{21} = -\alpha\beta\bar{B}_1 g,\quad C_{22} = -g\left(\bar{B}_2\alpha^2+\bar{B}_3\beta^2\right),\quad C_{23} = C_{24} = C_{25} = 0,\\
&C_{31} = C_{32} = 0,\quad C_{33} = -g\left(\bar{C}_1\alpha^2+\bar{C}_2\beta^2\right) - c_d\left(1+\mu\alpha^2+\mu\beta^2\right),\quad C_{34} = -\alpha\bar{C}_3 g,\quad C_{35} = -\beta\bar{C}_4 g,\\
&C_{41} = C_{42} = 0,\quad C_{43} = \alpha\bar{D}_1 g,\quad C_{44} = -g\left(\bar{D}_2\alpha^2+\bar{D}_3\beta^2-\bar{D}_4\right),\quad C_{45} = -\alpha\beta\bar{D}_5 g,\\
&C_{51} = C_{52} = 0,\quad C_{53} = \beta\bar{E}_1 g,\quad C_{54} = -\alpha\beta\bar{E}_2 g,\quad C_{55} = -g\left(\bar{E}_3\alpha^2+\bar{E}_4\beta^2-\bar{E}_5\right),
\end{aligned} \tag{B.2}$$

$$\begin{aligned}
&K_{11} = -\left(\bar{A}_1\alpha^2+\bar{A}_2\beta^2\right),\quad K_{12} = -\alpha\beta\bar{A}_3,\quad K_{13} = K_{14} = K_{15} = 0,\\
&K_{21} = -\alpha\beta\bar{B}_1,\quad K_{22} = -\left(\bar{B}_2\alpha^2+\bar{B}_3\beta^2\right),\quad K_{23} = K_{24} = K_{25} = 0,\\
&K_{31} = K_{32} = 0,\quad K_{33} = -\left(\bar{C}_1\alpha^2+\bar{C}_2\beta^2\right) - \begin{pmatrix} k_{g\xi}\left(\cos^2\theta\,\alpha^2 + 2\cos\theta\sin\theta\,\alpha\beta + \sin^2\theta\,\beta^2\right) \\ +k_{g\eta}\left(\sin^2\theta\,\alpha^2 - 2\sin\theta\cos\theta\,\alpha\beta + \cos^2\theta\,\beta^2\right) - k_w \end{pmatrix}\left(1+\mu\alpha^2+\mu\beta^2\right),\\
&K_{34} = -\alpha\bar{C}_3,\quad K_{35} = -\beta\bar{C}_4,\\
&K_{41} = K_{42} = 0,\quad K_{43} = \alpha\bar{D}_1,\quad K_{44} = -\left(\bar{D}_2\alpha^2+\bar{D}_3\beta^2-\bar{D}_4\right),\quad K_{45} = -\alpha\beta\bar{D}_5,\\
&K_{51} = K_{52} = 0,\quad K_{53} = \beta\bar{E}_1,\quad K_{54} = -\alpha\beta\bar{E}_2,\quad K_{55} = -\left(\bar{E}_3\alpha^2+\bar{E}_4\beta^2-\bar{E}_5\right),
\end{aligned} \tag{B.3}$$

REFERENCES

[1] Lee C., Wei X.D., Kysar J.W., Hone J., 2008, Measurement of the elastic properties and intrinsic strength of monolayer graphene, *Science* **321**: 385-388.

[2] Robinson J.T., Zalalutdinov M., Baldwin J.W., Snow E.S., Wei Z., Sheehan P., Houston B.H., 2008, Wafer-scale reduced graphene oxide films for nanomechanical devices, *Nano Letters* **8**: 3441-3445.

[3] Pisana S., Braganca P.M., Marinero E.E., Gurney B.A., 2010, Graphene magnetic field sensors, *IEEE Transactions on Magnetics* **46**: 1910-1913.

[4] Kuilla T., Bhadra S., Yao D., Kim N.H., Bose S., Lee J.H., 2010, Recent advances in graphene based polymer composites, *Progress in Polymer Science* **35**: 1350-1375.

[5] Ryzhii M., Satou A., Ryzhii V., Otsuji T., 2008, High-frequency properties of a graphene nanoribbon field-effect transistor, *Journal of Applied Physics* **104**: 114505.
[6] Murmu T., Adhikari S., 2013, Nonlocal mass nanosensors based on vibrating monolayer graphene sheets, *Sensors and Actuators B: Chemical* **188**: 1319-1327.
[7] Kuila T., Bose S., Khanra P., Mishra A.K., Kim N.H., Lee J.H., 2011, Recent advances in graphene-based biosensors, *Biosensors and Bioelectronics* **26**: 4637-4648.
[8] Sun X., Liu Z., Welsher K., Robinson J.T., Goodwin A., Zaric S., Dai H., 2008, Nano-graphene oxide for cellular imaging and drug delivery, *Nano Research* **1**: 203-212.
[9] Lam D.C.C., Yang F., Chong A.C.M., Wang J., Tong P., 2003, Experiments and theory in strain gradient elasticity, *Journal of the Mechanics and Physics of Solids* **51**: 1477-1508.
[10] Akgöz, B., Civalek Ö., 2012, Free vibration analysis for single-layered graphene sheets in an elastic matrix via modified couple stress theory, *Materials and Design* **42**: 164-171.
[11] Ghorbanpour Arani A., Abdollahian M., Jalaei M.H., 2015, Vibration of bioliquid-filled microtubules embedded in cytoplasm including surface effects using modified couple stress theory, *Journal of Theoretical Biology* **367**: 29-38.
[12] Eringen A.C., 2002, *Nonlocal Continuum Field Theories*, New York, Springer.
[13] Pradhan S.C., Murmu T., 2009, Small scale effect on the buckling of single-layered graphene sheets under biaxial compression via nonlocal continuum mechanics, *Computational Materials Science* **47**: 268-274.
[14] Hosseini Hashemi Sh., Tourki Samaei A., 2011, Buckling analysis of micro/nanoscale plates via nonlocal elasticity theory, *Physica E* **43**: 1400-1404.
[15] Shen H.S., 2011, Nonlocal plate model for nonlinear analysis of thin films on elastic foundations in thermal environments, *Composite Structures* **93**: 1143-1152.
[16] Ansari R., Rouhi H., 2012, Explicit analytical expressions for the critical buckling stresses in a monolayer graphene based on nonlocal elasticity, *Solid State Communications* **152**: 56-59.
[17] Mohammadi M., Ghayour M., Farajpour A., 2013, Free transverse vibration analysis of circular and annular graphene sheets with various boundary conditions using the nonlocal continuum plate model, *Composites: Part B* **45**: 32-42.
[18] Zenkour A.M., Sobhy M., 2013, Nonlocal elasticity theory for thermal buckling of nanoplates lying on Winkler–Pasternak elastic substrate medium, *Physica E* **53**: 251-259.
[19] Ghorbanpour Arani A., Maboudi M.J., Kolahchi R., 2014, Nonlinear vibration analysis of viscoelastically coupled DLAGS-system, *European Journal of Mechanics A/Solids* **45**: 185-197.
[20] Kananipour H., 2014, Static analysis of nanoplates based on the nonlocal Kirchhoff and Mindlin plate theories using DQM, *Latin American Journal of Solids and Structures* **11**: 1709-1720.
[21] Mohammadi M., Farajpour A., Goodarzi M., Shehni nezhad pour H., 2014, Numerical study of the effect of shear in-plane load on the vibration analysis of graphene sheet embedded in an elastic medium, *Computational Materials Science* **82**: 510-520.
[22] Golmakani M.E., Rezatalab J., 2014, Nonlinear bending analysis of orthotropic nanoscale plates in an elastic matrix based on nonlocal continuum mechanics, *Composite Structures* **111**: 85-97.
[23] Liu C.C., Chen Z.B., 2014, Dynamic analysis of finite periodic nanoplate structures with various boundaries, *Physica E* **60**: 139-146.
[24] Ghorbanpour Arani A., Jalaei M.H., 2015, Nonlocal dynamic response of embedded single-layered graphene sheet via analytical approach, *Journal of Engineering Mathematics* **92**: 129-144.
[25] Pouresmaeeli S., Ghavanloo E., Fazelzadeh S.A., 2013, Vibration analysis of viscoelastic orthotropic nanoplates resting on viscoelastic medium, *Composite Structures* **96**: 405-410.
[26] Karličić D., Kozić P., Pavlović R., 2014, Free transverse vibration of nonlocal viscoelastic orthotropic multi-nanoplate system (MNPS) embedded in a viscoelastic medium, *Composite Structures* **115**: 89-99.
[27] Wang Y., Li F.M., Wang Y.Z., 2015, Nonlinear vibration of double layered viscoelastic nanoplates based on the nonlocal theory, *Physica E* **67**: 65-76.
[28] Hosseini Hashemi Sh., Mehrabani H., Ahmadi-Savadkoohi A., 2015, Exact solution for free vibration of coupled double viscoelastic graphene sheets by viscoPasternak medium, *Composites Part B* **78**: 377-383.
[29] Reddy J.N., 2004, *Mechanics of Laminated Composite Plates and Shells: Theory and Analysis*, CRC Press, Boca Raton.
[30] Ghorbanpour Arani A., Shiravand A., Rahi M., Kolahchi R., 2012, Nonlocal vibration of coupled DLGS systems embedded on visco-Pasternak foundation, *Physica B* **407**: 4123-4131.
[31] Kutlu A., Uğurlu B., Omurtag M.H., Ergin A., 2012, Dynamic response on Mindlin plates resting on arbitrarily orthotropic Pasternak foundation and partially in contact with fluid, *Ocean Engineering* **42**: 112-125.
[32] Kiani Y., Sadighi M., Eslami M.R., 2013, Dynamic analysis and active control of smart doubly curved FGM panels, *Composite Structures* **102**: 205-216.
[33] Krylov V.I., Skoblya N.S., 1977, *A Handbook of Methods of Approximate Fourier Transformation and Inversion of the Laplace Transformation*, Moscow, Mir Publishers.
[34] Mohammadi M., Farajpour A., Goodarzi M., Heydarshenas., 2013, Levy type solution for nonlocal thermo-mechanical vibration of orthotropic mono-layer graphene sheet embedded in an elastic medium, *Journal of Solid Mechanics* **5**: 116-132.

[35] Thai H-T., Kim S-E., 2012, Analytical solution of a two variable refined plate theory for bending analysis of orthotropic Levy-type plates, *International Journal of Mechanical Sciences* **54**: 269-276.

[36] Reddy J.N., 2000, Analysis of functionally graded plates, *International Journal for Numerical Methods in Engineering* **47**: 663-684.